Environmental Science & Technology

pubs.acs.org/est

Article

Development and Validation of a Two-Stage Kinetic Sorption Model for Polymer and Surfactant Transport in Porous Media

Hamed Mohammadnejad, Shuchi Liao, Bonnie A. Marion, Kurt D. Pennell, and Linda M. Abriola*

Cite This: *Environ. Sci. Technol.* 2020, 54, 4912–4921

Read Online

ACCESS | Metrics & More | Article Recommendations | Supporting Information

ABSTRACT: Understanding the sorption processes is critical to the successful design and implementation of a variety of technologies in subsurface application. Most transport models assume minimal interactions between adsorbed species and, thus, are unable to accurately describe the formation of adsorbed bilayers. To address this limitation, a two-stage kinetic sorption model is developed and incorporated into a one-dimensional advective–dispersive–reactive transport simulator. The model is evaluated using data obtained from column experiments conducted with a representative polymer [gum arabic (GA)] and a nonionic surfactant [Witconol 2722 (WT)] under a range of experimental conditions. Model simulations demonstrate that the first-stage polymer/surfactant-surface sorption rate is at least 1 order of magnitude greater than the second-stage rate, associated with bilayer formation, indicating that the first-stage reaction is more favorable. The reversibility of the second-stage sorption process is found to be compound-specific, with irreversible sorption observed for GA and prolonged tailing observed for WT. This study demonstrates that the developed two-stage kinetic model is superior to a two-stage equilibrium-based model in its replication of two-leg breakthrough curves observed in core flood experiments; the normalized root-mean-square error between measurement and regressed model simulations was reduced by an average of 41% with the kinetic approach.

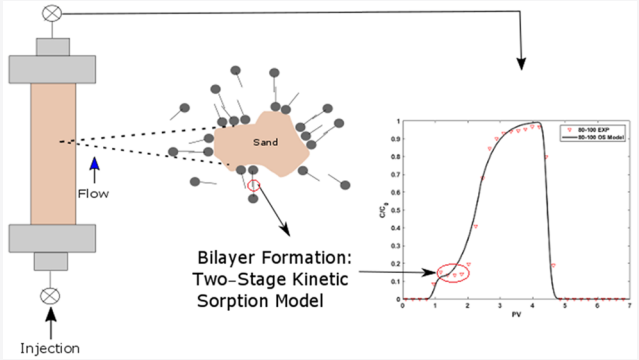

INTRODUCTION

The introduction of aqueous surfactant or polymer solutions has the potential to influence the subsurface transport behavior of bacteria, nanoparticles, and other dissolved solutes. Due to their unique surface-active properties, these compounds tend to adsorb onto mineral surfaces, altering the electrostatic, hydrophobic, and steric interactions between surfaces and solution constituents. Studies show that surfactants can adsorb to the surface of bacteria and facilitate transport by strengthening the repulsive force between sand grains and bacteria.[1−3] Surfactants can also be utilized as pesticide adjuvants to improve spreading on plant surfaces by reducing the surface tension of water.[4,5] In nanotechnology applications, surfactants or polymers can be introduced in a preflood or co-injected with a nanoparticle suspension to improve nanoparticle mobility[6,7] or can be used as coating agents to improve nanoparticle stability.[8−10] Surfactant and polymer addition has also been employed in both the environmental remediation and petroleum industries to alter viscosity, improve sweep efficiency, and enhance the recovery of organic liquids (e.g., oil or chlorinated solvents) from geological formations.[11−13] To assess the feasibility of using surfactants or polymers in a desired application and to explore the potential influence of these compounds on the environmental fate of dissolved solutes and nanoparticles, knowledge of coupled sorption and transport behavior is essential.

Water-soluble polymers widely used for subsurface applications[14] are generally classified as synthetic [e.g., hydrolyzed polyacrylamide (HPAM)] or biopolymers. Biopolymers, such as xantham gum or gum arabic (GA), typically consist of high-molecular weight (>200 kDa) polysaccharides. Surfactants, which constitute a special type of polymer, are generally classified as nonionic, anionic, cationic, or zwitterionic on the basis of the polarity of their headgroup.[15] A number of experimental studies have investigated nonionic surfactant sorption behavior and reported bilayer formation on mineral surfaces.[16−19] During bilayer formation, a polymer or surfactant first adsorbs onto the mineral surface in the absence of other adsorbed molecules.[20] At higher concentrations, once the adsorbed mass covers the mineral surface to form an adsorbed monolayer, interactions between the hydrophobic

Received: January 7, 2020
Revised: March 17, 2020
Accepted: March 27, 2020
Published: March 27, 2020

https://dx.doi.org/10.1021/acs.est.0c00123
Environ. Sci. Technol. 2020, 54, 4912–4921

Table 1. Properties of Porous Media and Associated Polymer Sorption Parameters[a]

porous medium	k_i (m^2)	d_{50} (μm)	SSA (m^2/g)	polymer	S_{max} (mg/g)	b (L/mg)	R^2	CSM (μg/g)
20−30 mesh OS	3.9×10^{-10}	725	0.010	WT	0.148	0.026	0.98	26.8
40−50 mesh OS	1.14×10^{-11}	335	0.013	GA	0.031	0.020	0.88	16.6
80−100 mesh OS	4.26×10^{-12}	160	0.019	GA	0.051	0.016	0.98	24.2
60−170 mesh CSS	5.40×10^{-13}	154	22.54	GA	1.033	0.001	0.95	272.0

[a]k_i is the intrinsic permeability. d_{50} is the particle size corresponding to 50% cumulative weight retained. SSA is the specific surface area.[6,36] S_{max} is the Langmuir maximum sorption capacity. b is the Langmuir sorption parameter. CSM is the sorbed mass at the monolayer. OS is Ottawa sand. WT is Witconol 2722. GA is gum arabic. CSS is crushed Berea sandstone.

moieties of surfactant monomers in solution and adsorbed surfactant molecules result in bilayer formation, often termed "second-stage" sorption.[21,22]

There is an extensive literature on the sorption of surfactants and polymers on mineral surfaces, encompassing both experimental and modeling investigations.[22−25] In this body of work, sorption is frequently treated as an equilibrium phenomenon,[26] where linear,[27] Langmuir,[28] or Freundlich[29] models are employed to represent the equilibrium distribution of surfactants and polymers between the aqueous and solid phases. A few studies have explored non-equilibrium sorption, which is typically modeled by incorporating mass transfer (diffusional) resistance from the bulk fluid to the solid surface.[30] In contrast, much less attention has been directed toward polymer−polymer interactions, presumably because these interactions tend to be negligible in dilute solutions. However, such interactions are important at higher concentrations, particularly near or above the critical micelle concentration (CMC).[31] To the best of our knowledge, the only mathematical model that has accounted for the influence of multilayer sorption on transport was presented by Adeel and colleagues.[17] They used a two-stage approach to describe the bilayer sorption behavior observed for a nonionic surfactant (Triton X-100) during transport through columns packed with Lincoln fine sand. In their model, the first sorption stage was considered rapid and irreversible, while the second stage was considered reversible, approaching equilibrium conditions. Although their model was able to fit the general rise of the experimental Triton X-100 breakthrough curves (BTCs) under most conditions, the model was unable to capture late-time tailing behavior or the observed stepped rise in effluent concentrations associated with the second-stage sorption process.

The objectives of this study were to develop and evaluate a general framework for modeling transport and retention of nonionic surfactants and polymers in porous media over a range of experimental conditions. Batch and column studies were performed with three size fractions of Ottawa sand (OS) (20−30, 40−50, and 80−100 mesh) and crushed Berea sandstone (CSS) (60−170 mesh) as the solid phases. The batch studies were used to quantify the equilibrium sorption capacity of a representative biopolymer (GA) and nonionic surfactant (Witconol 2722), while column experiments facilitated examination of sorption and transport behavior under dynamic conditions, for varying input concentrations and flow rates. Model simulations of effluent breakthrough concentration data were then used to assess the applicability of single- and two-stage sorption models and to estimate associated kinetic parameters. Model simulations illustrate the importance of sorption−desorption rate limitations and bilayer formation on polymer and surfactant transport behavior and explore the influence of hydrodynamic effects on polymer and surfactant desorption.

MATERIALS AND METHODS

Materials. Gum Arabic (GA), commonly used in the food industry as a stabilizing agent and emulsifier,[32] was purchased from Sigma-Aldrich (lot BCBJ3460V, 250 kDa; St. Louis, MO). GA is a biopolymer derived from the acacia tree, consisting of a mixture of glycoproteins and polysaccharides. Polyoxyethylene (20) sorbitan monooleate (lot B260), commonly known by the trade name Witconol 2722 (WT), was provided by the Witco Corp. and used as received without purification. The average molecular weight, critical micelle concentration (CMC), and hydrophilic−lipophilic balance (HLB) of WT are 1310 g/mol, 35 mg/L, and 15.0, respectively.[33]

The 20−30 mesh size fraction of OS (ASTM designation C778) was purchased directly from U.S. Silica (Berkeley Springs, WV), while the 40−50 and 80−100 mesh size fractions were obtained by sieving F-50 OS (U.S. Silica) with an RX-29 Ro-Tap sieve shaker (W. S. Tyler Inc., Mentor, OH). The 60−170 mesh size fraction of Berea sandstone was obtained from a block of Berea 400 sandstone (Cleveland Quarries, Vermilion, OH) that was crushed and sieved by StimLab Inc. (Duncan, OK). X-ray diffraction (XRD) analysis of OS indicated a silica content of >99%,[34] while XRD analysis of the Berea sandstone indicated a quartz content ranging from 83% to 88% and a clay content ranging from 5% to 7%, the latter including illite, chlorite, and kaolinite. The intrinsic permeability (k_i) of each porous medium was determined using a constant head permeameter following American Society for Testing and Materials (ASTM) method D2434-68.35.[35] Relevant properties of the porous media are summarized in Table 1.

Batch Sorption Studies. Batch sorption experiments were conducted in 35 mL glass centrifuge tubes with caps with polytetrafluoroethylene (PTFE)-backed septa. Approximately 30 g of air-dried OS (20−30 mesh, 40−50 mesh, and 80−100 mesh) or 10 g of crushed Berea sandstone (CSS) (60−170 mesh) was weighed into each centrifuge tube, to which an aqueous solution of WT or GA was added at an initial concentration ranging from 0 to 30 g/L in 3.6 mM NaCl. The contents of each centrifuge tube were mixed on a Burrell Wrist Action Shaker Model BB for 72 h at 22 ± 1 °C. The solid and aqueous phases were separated using an Eppendorf (Hamburg, Germany) 5804R benchtop centrifuge. All batch experiments were run in triplicate and included blanks that contained no solid phase.

Column Studies. Transport experiments were performed in borosilicate glass columns (2.5 cm diameter × 10.5 cm length or 4.8 cm diameter × 15 cm length, Kontes, Vineland, NJ) equipped with PTFE end plates fitted with a 40 mesh

https://dx.doi.org/10.1021/acs.est.0c00123
Environ. Sci. Technol. 2020, 54, 4912−4921

Table 2. Experimental Conditions and Fitted Parameters for Column Transport Studies Conducted with Gum Arabic (GA) and Witconol 2722 (WT)

	experiment	medium	θ_w[a]	injection concentration (mg/L)	Q[b] (mL/min)	pore velocity (m/day)	PV injected	α[c] (cm)
GA	1	40−50 OS	0.38	210	0.263	2.0	3.55	0.051
	2	80−100 OS	0.38	241.7	0.270	2.0	3.57	0.060
	3	60−170 CSS	0.42	909	0.262	2.0	3.22	0.051
	4	80−100 OS	0.38	100	0.27	2.0	3.59	0.060
	5			100	2.0	15	3.61	
	6			100	4.0	30	3.66	
	7			50	0.27	2.0	3.61	
	8			100	0.27	2.0	3.59	
	9			240	0.27	2.0	3.59	
WT	10	20−30 OS	0.34	98.3	0.99	2.2	2.99	0.053
	11			99.7	1.99	4.4	3.02	
	12			98.4	2.99	6.6	3.24	

[a]Volumetric water content. [b]Injection flow rate. [c]Hydrodynamic dispersivity.

nylon screen and a 70 μm nylon filter (Spectrum Laboratories Inc., Rancho Dominguez, CA). The columns were sterilized and packed with air-dry porous medium in 1 cm increments and flushed with CO_2 gas for at least 20 min to promote dissolution of entrapped air during the water imbibition process. Columns were then flushed with at least 10 pore volumes (PVs) of the background electrolyte solution (3.6 mM NaCl) prepared in degassed, deionized (DI) water and delivered in an up-flow mode at a rate of 1 mL/min using a Dynamax SD-200 pump (Varian Inc., Palo Alto, CA) equipped with a 25 mL pump head and a pulse dampener.

After each complete column saturation, approximately 3 PVs of a nonreactive tracer solution (3.6 mM NaBr), followed by approximately 3 PVs of the background electrolyte solution (3.6 mM NaCl), was injected in the up-flow direction using a model 22 syringe pump (Harvard Apparatus Inc., Holliston, MA). Column effluent samples were collected continuously in 15 mL sterile plastic centrifuge tubes (VWR International, Radnor, PA) with a CF-2 SpectraChrom fraction collector (Spectrum Laboratories Inc.). Nonreactive tracer breakthrough curves were plotted as relative concentration (C/C_o, where C_o is the influent or applied concentration and C is the measured effluent concentration) versus the number of dimensionless PVs of the influent solution introduced into the column.[36] These data were fit to a one-dimensional form of the advective−dispersive−reactive (ADR) transport equation using the CXTFIT model, version 2.1,[37] to obtain hydrodynamic dispersivity values (α) that ranged from 0.051 to 0.060 cm, with retardation factors (R_F) of 0.99−1.02. Immediately after the nonreactive tracer test, a pulse (~3.5 PVs) of either the WT solution (~100 mg/L) or the GA solution (~250−900 mg/L) was introduced into each column. Surfactant or polymer concentrations present in aquifer formations can vary over a very wide range, from rather dilute (<100 mg/L) to 50000 mg/L, depending upon the use or release scenario. Here, concentrations were selected to create mass loadings that would facilitate investigation of sorption processes below the maximum sorption capacity. Injection flow rates in the column experiments ranged from 0.26 to 2.99 mL/min. This range was selected to represent flow in relatively high permeability aquifer materials (quartz sands) under natural gradient conditions and pumping/injection conditions. Experimental parameters for the suite of column experiments are provided in Table 2. Note that for experiment 3, conducted with CSS, the injection concentration was increased to ~900 mg/L to ensure polymer breakthrough due to the larger specific surface area (SSA) of this porous medium.

Analytical Methods. Bromide tracer concentrations were measured using an ion-selective bromide electrode (Cole-Parmer Instrument Co., Vernon Hills, IL) connected to an Accumet model 50 pH meter (Fisher Scientific, Fair Lawn, NJ). Quantification of WT was performed using a Cary 3E UV−vis spectrophotometer operated at a wavelength of 234 nm. A five-point calibration curve was prepared over a concentration range of 0−200 mg/L, which yielded a linear relationship with a regression coefficient (r^2) of 0.97. Quantification of GA was performed using a Shimadzu Total Organic Carbon Analyzer model TOC-L series with Autosampler ASI-L (Shimadzu Scientific Instruments, Columbia, MD). To construct a calibration curve, GA solutions (0−100 mg/L) were prepared and diluted 2-fold with a 5 mM H_2SO_4 solution, which resulted in a linear curve with an r^2 value of >0.99 with a detection limit of 0.9 mg/L. All GA measurements were performed in triplicate.

MATHEMATICAL MODELING

A conceptual model of the two-stage sorption process is presented in Figure S1. First-stage sorption occurs when the amount of sorbed polymer is less than the monolayer coverage and molecules are assumed to be oriented parallel to the solid surface.[17] At higher sorbed mass concentrations, the hydrophobic moieties of the polymers begin to reorient, becoming perpendicular to the solid surface. This realignment is attributed to mutual attraction between the hydrophobic moieties of adjacent polymer molecules.[21] Second-stage sorption occurs when the hydrophobic moieties of the adsorbed and aqueous polymer molecules interact to form a bilayer.

In this work, two alternative approaches for mathematical modeling of the two-stage sorption process were evaluated. These approaches differ in their representation of second-stage sorption. In the two-stage equilibrium-based (TSE) model, consistent with the mathematical formulation presented in Adeel et al.,[17] a completely reversible, quasi-equilibrium, condition is assumed for the second stage. The second approach, which is developed herein, is termed the two-stage kinetic model (TSK). The TSK model incorporates independent sorption and desorption rates for the second stage and accounts for inhibition resulting from occupied sorption sites during the second-stage sorption.

https://dx.doi.org/10.1021/acs.est.0c00123
Environ. Sci. Technol. 2020, 54, 4912−4921

Both models are predicated on the same mass balance equation, a traditional one-dimensional ADR equation:

$$\frac{\partial C}{\partial t} + \frac{\rho_b}{\theta_w}\frac{\partial S}{\partial t} = D_H\frac{\partial^2 C}{\partial x^2} - v_p\frac{\partial C}{\partial x} \quad (1)$$

where C is the concentration of the polymer in the aqueous phase (M/L^3), S is the sorbed mass on the solid surface (M/M), D_H is the hydrodynamic dispersion coefficient (L^2/T), v_p (L/T) is the pore water velocity, ρ_b is the bulk density (M/L^3), and θ_w is the volumetric water content of the porous medium. Here, the second term on the left-hand side of eq 1 accounts for changes in the aqueous phase concentration due to sorption by the solid phase. Here, a homogeneous packing is assumed and microbial transformation is neglected, consistent with experimental conditions.

Conceptually, each sorption stage can be represented as a first-order rate process, parametrized by constant sorption and desorption rate parameters, k_a and k_d, respectively (T^{-1}). For stage 1, the sorption rate corresponds to the interaction between the polymer and the mineral surface, whereas the sorption process in stage 2 is controlled by polymer−polymer interactions:

$$C \underset{k_{d,1}}{\overset{k_{a,1}}{\rightleftarrows}} S \text{ when } S \le CSM \quad (2)$$

$$C \underset{k_{d,2}}{\overset{k_{a,2}}{\rightleftarrows}} S \text{ when } S > CSM \quad (3)$$

Here, subscripts 1 and 2 indicate the sorption stage. The first reaction is applicable up to the point at which the sorbed polymer occupies all available sites. During this first stage, the sorbed mass is below the critical sorbed mass (CSM) (eq 2), corresponding to the monolayer surface coverage.

On the basis of eq 2, the first-stage sorption term can be expressed as

$$\frac{\rho_b}{\theta_w}\frac{\partial S}{\partial t} = k_{a,1}C \text{ when } S \le CSM \quad (4)$$

Here, consistent with experimental observations indicating that first-stage sorption is rapid and irreversible,[38] the desorption rate ($k_{d,1}$) is assumed to be negligible. In contrast, the second-stage sorption process is assumed to be reversible, incorporating both sorption and desorption rate parameters. Thus, for sorbed phase concentrations that are greater than the CSM

$$\frac{\rho_b}{\theta_w}\frac{\partial S}{\partial t} = k_{a,2}C - k_{d,2}\frac{\rho_b}{\theta_w}(S - CSM) \text{ when } S > CSM \quad (5)$$

where the term $S - CSM$ is the amount of sorbed mass attributed to second-stage sorption. Using the CSM cutoff to distinguish sorption stages is a simplifying assumption. In reality, the transition between these two stages may not be sharp and bilayer formation could begin before full monolayer coverage is achieved.[21]

The two alternative modeling approaches differ in their treatment of the rate coefficients in eq 5. The TSE model employs a quasi-equilibrium assumption to further simplify the second-stage sorption expression.[17] At equilibrium, the sorption rate coefficient can be expressed in terms of the desorption rate coefficient:

$$k_{a,2} = k_{d,2}\frac{\rho_b(S_{eq} - CSM)}{\theta_w C} \quad (6)$$

where S_{eq} is the sorbed phase concentration at equilibrium (M/M). If second-stage sorption is assumed to approach equilibrium, $k_{a,2}$ in eq 6 can be incorporated into eq 5 to achieve a modified linear driving force expression for the second-stage sorption term:

$$\frac{\rho_b}{\theta_w}\frac{\partial S}{\partial t} = -k_{d,2}\frac{\rho_b}{\theta_w}(S_{eq} - S) \quad (7)$$

The equilibrium sorption capacity, S_{eq}, is assumed to follow a Langmuir isotherm, consistent with experimental data available for polymer and surfactant sorption:[39]

$$S_{eq} = \frac{bCS_{max}}{1 + bC} \quad (8)$$

where S_{max} is the maximum sorption capacity (M/M) and b is the affinity constant (L^3/M).

In the TSK model, a fully kinetic formulation is employed with both sorption and desorption rate parameters. A limiting sorption capacity is incorporated by introducing an inhibition factor, Ψ_m, into the second-stage sorption expression. The inhibition factor moderates the sorption rate as a function of available sorption sites. As more polymers are sorbed in the second stage, active sorption sites become scarcer, resulting in a reduction in the second-stage adsorption rate ($k_{a,2}$). This factor has the same mathematical form as that which has been used successfully to model a limiting attachment capacity in nanoparticle and colloid attachment studies.[40] The second-stage sorption expression for the TSK model is given as

$$\frac{\rho_b}{\theta_w}\frac{\partial S}{\partial t} = k_{a,2}\Psi_m C - k_{d,2}\frac{\rho_b}{\theta_w}(S - CSM) \text{ when } S > CSM \quad (9a)$$

where

$$\Psi_m = 1 - \frac{S - CSM}{S_{eq} - CSM} \quad (9b)$$

Here, Ψ_m ranges from 0 to 1, where a value of 1 corresponds to the beginning of second-stage sorption and a value of 0 is achieved when sorption reaches the maximum capacity.

The equations presented above were implemented in a finite difference simulator. A third type of boundary condition ($D_H\frac{dC}{dx} + v_pC = v_pC_{injection}$) was imposed at the column inlet, while a no dispersive flux boundary condition was implemented at the outlet. The mass balance equation (eq 1) was discretized using a semi-implicit central weighted algorithm. The two alternative two-stage sorption models are described by eqs 1, 4, 7, and 8 (TSE model) and eqs 1, 4, 8, and 9 (TSK model). At each time step, the transport equation was solved implicitly for aqueous polymer or surfactant concentration using the value of the sorbed mass obtained from the previous time step. The value for sorbed mass, S, was then updated using an explicit, discretized, form of a sorption equation selected on the basis of the stage of sorption and the chosen two-stage model. When $S \le CSM$, the explicit form of the first-stage equation (eq 4) was employed; otherwise, eq 7 or 9 was used to update the S value. Computational domains were divided into 100 grid cells, and time step sizes were chosen to satisfy local and global mass balance criteria and a

https://dx.doi.org/10.1021/acs.est.0c00123
Environ. Sci. Technol. 2020, 54, 4912−4921

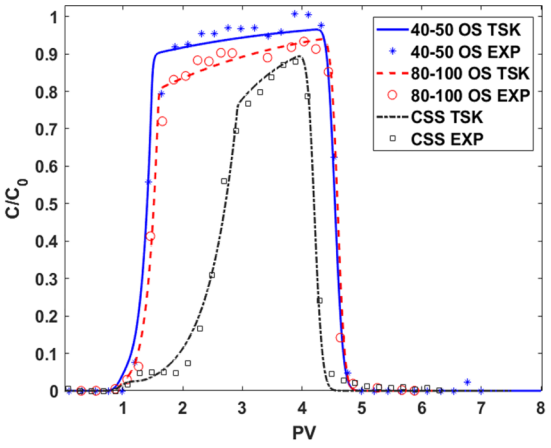

a) Influence of Porous Medium, experiments 1-3, TSK model

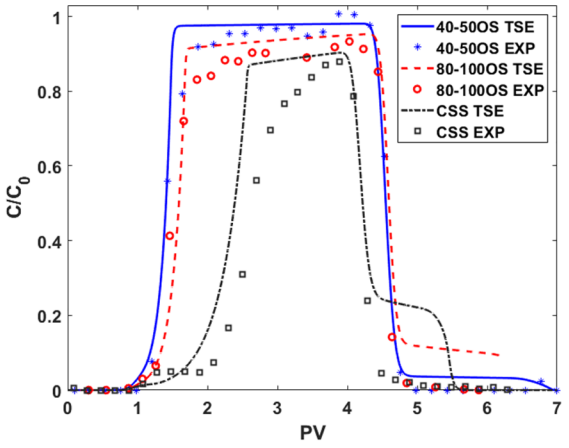

b) Influence of porous medium, experiments 1-3, TSE model

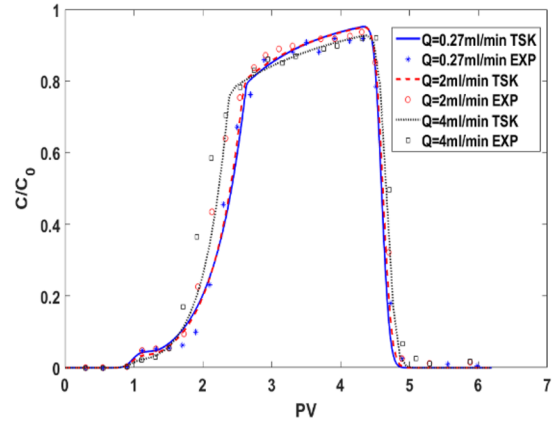

c) Influence of flow rate, experiments 4-6, TSK model

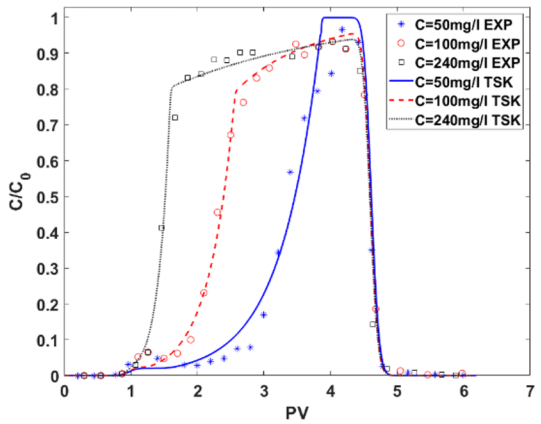

d) Influence of influent concentration, experiments 7-9, TSK model

Figure 1. Comparison of experimental observations and fitted model simulations for GA BTCs in three different porous media using the (a) TSK and (b) TSE models. Effect of (c) flow rate and (d) influent concentration in the TSK model.

Courant condition of Cr < 0.1, where Cr = $v_p\Delta x/\Delta t$ (Δx and Δt are the grid and time step size, respectively). The solutions presented herein had <0.01% global mass balance error.

Parameter Estimation. Application of the two-stage sorption models requires an estimate of the CSM, which is assumed to be equivalent to the sorbed mass at monolayer surface coverage. To obtain an independent estimate of monolayer coverage for each polymer/porous medium combination, the surface coverage concept was employed.[21,41] In this approach, the estimated mineral surface area occupied by a molecule of GA or WT oriented parallel to the surface was used (see the Supporting Information) in conjunction with the measured SSA of the porous medium to obtain CSM values (Table 1):

$$\mathrm{CSM} = \frac{\mathrm{SSA} \times \mathrm{MW}}{N_A A_P} \tag{10}$$

where MW is the molecular weight of the polymer, N_A is Avogadro's number, and A_P is the projected area of the adsorbed polymer on the surface. In an alternative approach, the BTC data can be used to estimate the CSM. Here, the sorbed mass of the polymer or surfactant at the first stage can be estimated by determining the area above and to the left of the BTC prior to the inflection point, which corresponds to the point in the BTC where monolayer coverage is achieved.[17] The details of these calculations are provided in the Supporting Information.

Sorption and desorption rate parameters (eqs 4 and 7 for TSE and eqs 4 and 9 for TSK models) were estimated by fitting model concentration predictions (C_{pred}) to experimental BTCs (C_{exp}) using a least-squares optimization procedure [MATLAB R2010a (The MathWorks, Natick, MA) function lsqnonlin] with the following objective function (note that all data points were given equal weight):

$$f(x) = \sum (C_{exp} - C_{pred})^2 \tag{11}$$

RESULTS AND DISCUSSION

Batch Sorption Studies. For all four porous media examined, sorption of GA and WT was rapid at low concentrations and exhibited a limiting or maximum sorption capacity at higher concentrations, consistent with the Langmuir isotherm model. The Langmuir expression (eq 8) was fit to the measured sorption data using a nonlinear, least-squares regression procedure to obtain independent estimates of the Langmuir isotherm constants, b and S_{max} (Table 1). These values are comparable with other surfactant sorption data reported in the literature, for example, Triton X-100 on Lincoln fine sand (b = 0.0015 L/mg, and S_{max} = 0.158 mg/g) and WT on 20−30 OS (b = 0.156 L/mg, and S_{max} = 4.06 mg/

https://dx.doi.org/10.1021/acs.est.0c00123
Environ. Sci. Technol. 2020, 54, 4912−4921

Table 3. Quasi-equilibrium (TSE) and Kinetic (TSK) Modeling Results for GA and WT Column Injection Experiments, Including Fitted Model Rate Parameters, Effluent Mass Recovery Values, and Model Goodness of Fit Values

experiment	mass recovery in effluent (%)	$k_{a,1}$[a] (h^{-1}) in the TSK model	$k_{a,2}$[a] (h^{-1}) in the TSK model	$k_{d,2}$[a] (h^{-1}) in the TSK model	NRSME[b] (%) for the TSK model	$k_{a,1}$[c] (h^{-1}) in the TSE model	$k_{d,2}$[c] (h^{-1}) in the TSE model	NRSME[b] (%) for the TSE model
1	85.0	2.11	0.09	–	3.20	2.30	0.07	4.82
2	76.5	2.13	0.17	–	4.90	1.98	0.08	8.73
3	45.4	2.93	0.35	–	3.04	2.91	0.17	15.32
4	59.5	1.79	0.16	–	4.07	1.22	0.12	8.32
5	63.8	13.1	1.18	–	3.70	12.6	0.67	7.05
6	66.4	30.9	2.31	–	6.38	28.08	1.34	9.02
7	34.7	2.27	0.22	–	5.95	2.21	0.22	5.98
8	59.5	1.82	0.18	–	2.68	1.77	0.12	7.12
9	76.3	1.97	0.16	–	4.96	2.01	0.08	8.45
10	NA	1.18	0.43	0.02	10.30	1.09	0.25	20.27
11	NA	3.28	0.44	0.43	4.37	3.56	0.10	4.41
12	NA	5.04	0.59	0.87	3.38	3.45	0.066	4.43

[a]Fitted rates of sorption and desorption in TSK model. [b]NRSME: Normalized Root Mean Squared Error: $\frac{\text{RSME}}{y\text{max} - y\text{min}}$. [c]Fitted rates of sorption and desorption in TSE model.

g).[17,42] Representative sorption data and Langmuir isotherm fits are presented in Table S1.

Gum Arabic Column Studies. Three independent column experiments (experiments 1–3 in Table 2) were conducted to evaluate the influence of porous media type on the sorption and transport behavior of GA in columns packed with 40–50 and 80–100 OS and CSS. Figure 1a shows the measured effluent BTCs for these experiments, plotted as the relative effluent concentration (C/C_o) versus the number of dimensionless PVs applied. Inspection of the figure reveals that no tailing was observed in the elution curve of any of the experiments, indicating the absence of rate-limited desorption.

Consistent with the conceptual model of a two-stage sorption process, the GA BTCs for the two finer-grained media (80–100 OS and CSS) exhibit an initial plateau or shelf. However, no initial plateau is visible for the 40–50 OS experiment (1). The absence of a plateau is attributed to the larger grain size and smaller SSA of this porous medium, which corresponds to a lower CSM value (16.6 μg/g in Table 1).

TSK model fits to the measured BTCs are presented as solid lines in Figure 1a. Here, two rate parameters were fit, the first-stage sorption rate ($k_{a,1}$) and the second-stage sorption rate ($k_{a,2}$). The second-stage desorption rate was set to zero, consistent with the absence of tailing. Fitted rate parameters and goodness of fit statistics are presented in Table 3. Inspection of Figure 1a indicates that the TSK model accurately reproduced the experimental BTCs, as indicated by the goodness of fit statistic (Table 3).

Two-parameter ($k_{a,1}$ and $k_{d,2}$) model fits were also undertaken for experiments 1–3 using the TSE model (Figure 1b). Here, as a consequence of the assumption of reversible second-stage sorption (quasi-equilibrium sorption), the TSE model was unable to capture the observed absence of second-stage desorption and predicted substantial tailing, which is reflected in the poorer normalized root-mean-square error (NRMSE) statistic (Table 3). Notice that the presence of a second-stage inhibition factor Ψ_m in the TSK model facilitates an improved fit to the observed BTC shape (approach to peak concentration). With the inclusion of Ψ_m (eq 9), the second-stage sorption rate decreases as sorption sites are filled. This decrease in sorption rate is associated with an increased level of polymer transport, increasing the height of the BTC as it approaches its peak. Additional model fits for GA experiments revealed a similar superiority of the TSK over the TSE model (Figure S3).

Three column experiments (experiments 4–6 in Table 2) were designed to investigate the effect of flow rate on GA transport behavior. The resulting BTCs demonstrate little sensitivity to the flow rate for either first- or second-stage sorption (Figure 1c). A slightly shorter shelf was observed at the highest flow rate. This low sensitivity may be attributed to a "shadow zone effect",[43] which has been observed in colloidal attachment studies in packed beds.[44,45] The shadow zone is a deposition exclusion area located on the down-gradient side of the collectors (grains), which grows with an increase in velocity and is associated with the combined effects of hydrodynamic interactions and double-layer repulsion. Also, as expected and consistent with the colloid transport literature,[7] a plot of the fitted first- and second-stage sorption rates reveals a linear relationship with flow rate (R^2 = 0.99) (see Figure S4).

To investigate the effects of concentration on the shape of the BTCs, three influent GA concentrations (50, 100, and 240 mg/L) were applied to columns packed with 80–100 OS, while all other conditions were unchanged (experiments 7–9 in Figure 1d). Here, the breakthrough time decreased with an increase in concentration, consistent with isotherm nonlinearity; i.e., once the adsorption capacity is reached, no additional loss to the solid phase will occur. Also observe that, as the influent concentration decreased, the height of the first-stage shelf decreased slightly, and the shelf became longer and more visible (Figure 1d). This behavior is attributed to the fact that a larger injected volume (i.e., more mass) is required to fill the first stage (monolayer) at a lower concentration. Note that sorption kinetics were not affected by the change in influent concentration; fitted rate parameters for the first- and second-stage sorption rates in the TSK model were consistent (< ±18%) across all experiments (Table 3). This similarity in sorption rate parameters supports the proposed two-stage sorption model and provides evidence for the uniqueness of model fits.

For all GA column experiments (experiments 1–9 in Table 3), the fitted sorption rate constants for the first-stage sorption process were 1 order of magnitude larger than those obtained for the second-stage sorption, indicating that the first stage is

https://dx.doi.org/10.1021/acs.est.0c00123
Environ. Sci. Technol. 2020, 54, 4912–4921

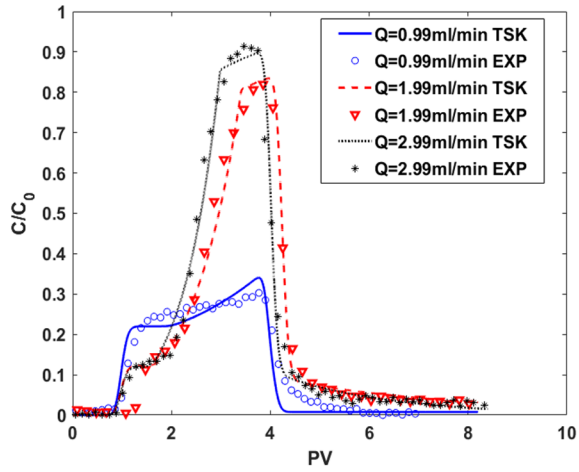

(a) WT transport: influence of flow rate in TSK model, experiments 10-12.

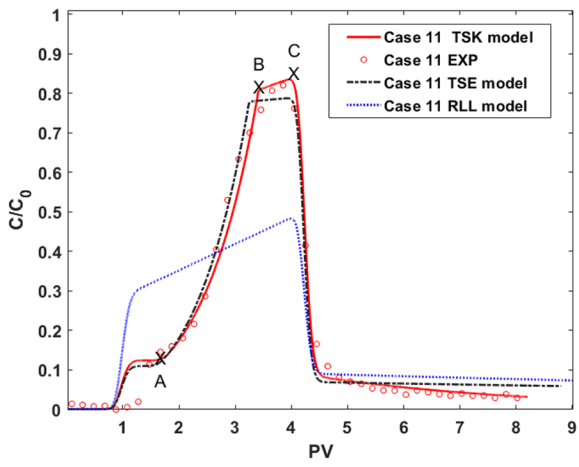

(b) Comparison of TSK, TSE and Langmuir Rate Limited models in experiment 11.

Figure 2. (a) Comparison of experimental observations and fitted model simulations for WT BTCs at three different flow rates. (b) Sorption regimes and model comparison for WT experiment 11. From 0 PV to point A, only first-stage sorption occurs. The inflection point of the curve (point A) is the point where the maximum sorption capacity of the first stage is reached. Between points A and B, second-stage sorption dominates in different areas of the column. Between points B and C, both second-stage sorption and desorption dominate. The surfactant injection stops at the PV indicated by point C, and flushing continues with the background solution.

much faster and more favorable for sorption than the second stage.

Witconol 2722 Column Studies. Column experiments were also undertaken to investigate the effect of multistage sorption on the transport behavior of a nonionic surfactant (WT) as a function of flow rate in 20−30 OS (experiments 10−12 in Table 2). Unlike the results for GA (Figure 1c), the WT BTCs (Figure 2a) exhibited much greater sensitivity to flow rate. In experiment 10, with the lowest flow rate (0.99 mL/min), the surfactant mass recovered in the effluent was much smaller than that observed in experiments 11 and 12. In addition, a significant amount of tailing was observed, particularly at the higher flow rates. This sensitivity to flow rate can be attributed to the trade-off between polymer−polymer interaction forces in the bilayer (van der Waals attraction) and drag forces.[46] Weaker polymer−polymer interactions in the second stage are expected to cause more sensitivity to flow rate and may increase the likelihood of desorption.

A comparison of fitted TSK model sorption rate coefficients for experiments 10−12 (Table 3) indicates that the first-stage sorption rate was faster than the second-stage sorption rate, similar to the results obtained for GA. Also similar to GA, a linear relationship exists between the first-stage sorption rates and flow rate (Figure S4). However, in contrast with GA experiments, no significant relationship was found between WT second-stage sorption rates and flow rate (see section D of the Supporting Information for statistical analysis).

Consistent with the observations of tailing in these experiments, second-stage desorption rates for WT were found to increase with an increase in flow rate. This behavior may be associated with the effect of hydrodynamic forces on surfactant−surfactant interactions occurring in the second sorption stage, where an increasing flow rate increases the drag force on sorbed polymers. Sabatini et al.[38] investigated the effect of flow rate on rhodamine transport and concluded that the mechanism of first-stage sorption, unlike the second stage, is not affected by flow rate (i.e., was not kinetically limited), consistent with the results of WT transport in this study.

Figure 2b presents a comparison of TSE and TSK model fits for an example WT column experiment (experiment 11). Here, unlike the comparisons observed for GA transport, both models accurately captured the two-stage sorption process. This finding is attributed to the presence of second-stage desorption in the WT experiments, which is consistent with the reversible second-stage sorption assumption of the TSE model. However, the slope of the tailing part of the curve (after point C in Figure 2b) was captured better by the TSK model, attributed to the inclusion of a desorption rate parameter. Similar to the behavior observed in the GA transport modeling examples, the TSK model more accurately represented the shape of the effluent BTC at the peak concentration (points B and C in Figure 2b), when second-stage sorption dominates. As with GA, this improvement in the TSK fit is attributed to the incorporation of an inhibition factor. Despite their differences, it is important to note that the TSE and TSK models perform significantly better than single-stage kinetic sorption models, using the same isotherm data. For example, Figure 2b presents a comparison of TSK and TSE model fits with that of a single-stage rate-limited Langmuir (RLL) model for experiment 11 BTC data. The RLL model is unable to replicate either the inflection point or the peak concentration of the BTC.

In summary, for both WT and GA experiments, TSK model fits were consistently better than those obtained with the TSE model (see Table 3). Incorporation of an inhibition factor in the second stage sorption model provided the ability to capture the observed S-shaped BTC corresponding to second-stage sorption. Addition of a desorption rate parameter was found to be necessary to replicate the observed tailing behavior of WT transport. The reversibility of the sorption process in the second stage was shown to depend on polymer type; while GA sorption was irreversible for all media examined, WT transport exhibited substantial tailing, attributed to drag forces acting on the sorbed bilayer. A linear relationship between the sorption

https://dx.doi.org/10.1021/acs.est.0c00123
Environ. Sci. Technol. 2020, 54, 4912−4921

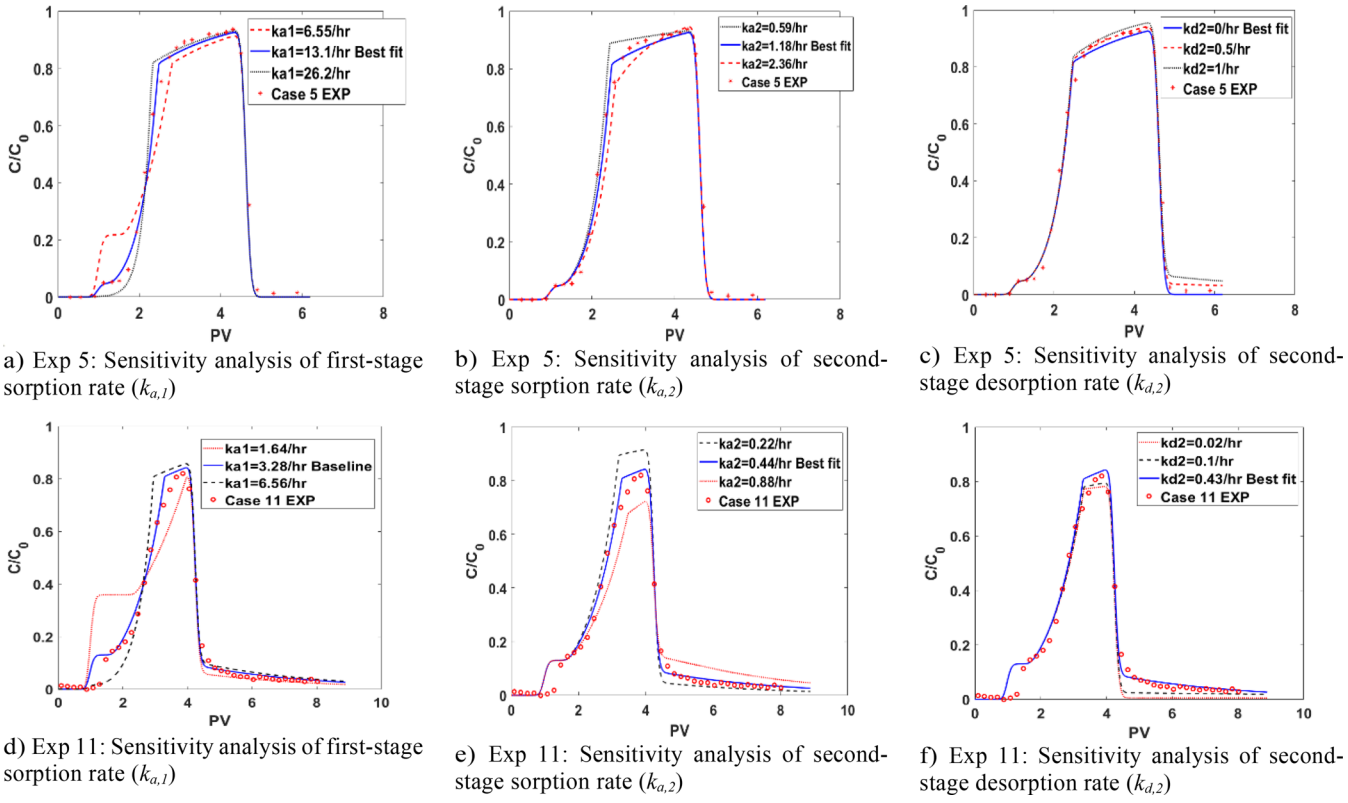

a) Exp 5: Sensitivity analysis of first-stage sorption rate ($k_{a,1}$)

b) Exp 5: Sensitivity analysis of second-stage sorption rate ($k_{a,2}$)

c) Exp 5: Sensitivity analysis of second-stage desorption rate ($k_{d,2}$)

d) Exp 11: Sensitivity analysis of first-stage sorption rate ($k_{a,1}$)

e) Exp 11: Sensitivity analysis of second-stage sorption rate ($k_{a,2}$)

f) Exp 11: Sensitivity analysis of second-stage desorption rate ($k_{d,2}$)

Figure 3. Sensitivity analysis of selected experiments with GA and WT (experiments 5 and 11).

rate coefficient and flow rate was observed for all experiments except for WT second-stage sorption. The anomalous behavior of WT may be due to the greater sensitivity of WT second-stage sorption to flow rate, attributed to weaker van der Waals attraction forces between polymer bilayers.

SENSITIVITY ANALYSIS

Experiments 5 (GA) and 11 (WT) were selected to illustrate the sensitivity of the shape of the BTC to variations in TSK model parameters (Figure 3). Panels a and d of Figure 3 illustrate the effect of variations in the first-stage sorption rate on GA and WT BTCs, respectively. Here, BTCs with best fit values of $k_{a,1}$ are compared with simulations employing a higher and lower value of $k_{a,1}$ ($2k_{a,1}$ and $0.5k_{a,1}$, respectively). Other rate parameters were kept constant, equal to the fitted values presented in Table 3. Inspection of the figures reveals that $k_{a,1}$ has a significant influence on the height and length of the effluent concentration shelf (first plateau) for both GA and WT. This behavior can be explained by the fact that, as the adsorption rate increases, the sorbed mass at a particular time increases, and thus, fewer PVs of the injected solution are needed to achieve monolayer coverage.

The second column experiment modeled in Figure 3 (Figure 3b,e) illustrates the influence of the second-stage sorption rate, $k_{a,2}$. Here, the value of $k_{a,2}$ was varied by a factor of 2 above and below the best fit case. Inspection of panels b and e of Figure 3 reveals that the second-stage sorption rate influences the shape of the approach to the concentration peak, its height, and the extent of BTC tailing. The shape of the first effluent concentration shelf is not affected by changes in $k_{a,2}$. However, increasing $k_{a,2}$ leads to an increase in the slope to the peak, a decrease in peak height, and an increase in tailing concentration. This behavior can be explained by the fact that the higher sorption rate results in an increased sorbed mass and lower effluent concentrations (lower peak height in the second stage). As expected, an increase (Figure 3c) or decrease (Figure 3f) in the desorption rate, $k_{d,2}$, increases or decreases, respectively, the observed tailing of the BTC. Results of the sensitivity analysis demonstrate the importance of incorporating rate-limited, two-stage sorption processes to reproduce observed features of polymer and surfactant BTCs.

ASSOCIATED CONTENT

Supporting Information

The Supporting Information is available free of charge at https://pubs.acs.org/doi/10.1021/acs.est.0c00123.

Monolayer coverage calculation (section A), batch sorption experiments to estimate Langmuir isotherm parameters (section B), additional GA BTC results using the TSE model (section C), statistical analysis of effects of flow rate on sorption (section D), and sensitivity analysis of CSM and S_{max} (section E) (PDF)

AUTHOR INFORMATION

Corresponding Author

Linda M. Abriola − *Department of Civil and Environmental Engineering, Tufts University, Medford, Massachusetts 02155, United States;* orcid.org/0000-0003-2420-6145; Email: Linda.abriola@tufts.edu

Authors

Hamed Mohammadnejad − *Department of Civil and Environmental Engineering, Tufts University, Medford, Massachusetts 02155, United States;* orcid.org/0000-0002-6185-8030

https://dx.doi.org/10.1021/acs.est.0c00123
Environ. Sci. Technol. 2020, 54, 4912−4921

Shuchi Liao − *School of Engineering, Brown University, Providence, Rhode Island 02912, United States*
Bonnie A. Marion − *Department of Civil and Environmental Engineering, Tufts University, Medford, Massachusetts 02155, United States*
Kurt D. Pennell − *School of Engineering, Brown University, Providence, Rhode Island 02912, United States;* orcid.org/0000-0002-5788-6397

Complete contact information is available at: https://pubs.acs.org/10.1021/acs.est.0c00123

Notes

The authors declare no competing financial interest.

■ ACKNOWLEDGMENTS

The authors thank Jae Jin (Lisa) Han for her assistance with the permeability measurments and column experiments. This work was supported by the Advanced Energy Consortium (www.beg.utexas.edu/aec) under Project BEG13-01 with ExxonMobil, Repsol, and Total as members.

■ REFERENCES

(1) Brown, D. G.; Jaffé, P. R. Effects of nonionic surfactants on bacterial transport through porous media. *Environ. Sci. Technol.* **2001**, *35* (19), 3877−3883.
(2) Gross, M. J.; Logan, B. E. Influence of different chemical treatments on transport of Alcaligenes paradoxus in porous media. *Appl. Environ. Microbiol.* **1995**, *61* (5), 1750−1756.
(3) Li, Q.; Logan, B. E. Enhancing bacterial transport for bioaugmentation of aquifers using low ionic strength solutions and surfactants. *Water Res.* **1999**, *33* (4), 1090−1100.
(4) Krogh, K.; Halling-Sørensen, B.; Mogensen, B.; Vejrup, K. Environmental properties and effects of nonionic surfactant adjuvants in pesticides: a review. *Chemosphere* **2003**, *50* (7), 871−901.
(5) Wang, C.; Liu, Z. Foliar uptake of pesticides—present status and future challenge. *Pestic. Biochem. Physiol.* **2007**, *87* (1), 1−8.
(6) Kmetz, A. A.; Becker, M. D.; Lyon, B. A.; Foster, E.; Xue, Z.; Johnston, K. P.; Abriola, L. M.; Pennell, K. D. Improved mobility of magnetite nanoparticles at high salinity with polymers and surfactants. *Energy Fuels* **2016**, *30* (3), 1915−1926.
(7) Wang, Y.; Becker, M. D.; Colvin, V. L.; Abriola, L. M.; Pennell, K. D. Influence of residual polymer on nanoparticle deposition in porous media. *Environ. Sci. Technol.* **2014**, *48* (18), 10664−10671.
(8) Godinez, I. G.; Darnault, C. J. Aggregation and transport of nano-TiO2 in saturated porous media: effects of pH, surfactants and flow velocity. *Water Res.* **2011**, *45* (2), 839−851.
(9) Sharma, K. P.; Aswal, V. K.; Kumaraswamy, G. Adsorption of nonionic surfactant on silica nanoparticles: structure and resultant interparticle interactions. *J. Phys. Chem. B* **2010**, *114* (34), 10986−10994.
(10) Alexeev, V.; Ilekti, P.; Persello, J.; Lambard, J.; Gulik, T.; Cabane, B. Dispersions of silica particles in surfactant phases. *Langmuir* **1996**, *12* (10), 2392−2401.
(11) Pennell, K. D.; Cápiro, N. L.; Walker, D. I. Surfactant and cosolvent flushing. In *Chlorinated Solvent Source Zone Remediation*; Springer, 2014; pp 353−394.
(12) Pennell, K. D.; Jin, M.; Abriola, L. M.; Pope, G. A. Surfactant enhanced remediation of soil columns contaminated by residual tetrachloroethylene. *J. Contam. Hydrol.* **1994**, *16* (1), 35−53.
(13) Shah, D. O. *Improved oil recovery by surfactant and polymer flooding*; Elsevier, 2012.
(14) Wever, D.; Picchioni, F.; Broekhuis, A. Polymers for enhanced oil recovery: a paradigm for structure−property relationship in aqueous solution. *Prog. Polym. Sci.* **2011**, *36* (11), 1558−1628.
(15) Rosen, M. J.; Kunjappu, J. T. *Surfactants and interfacial phenomena*; John Wiley & Sons, 2012.
(16) Paria, S. Surfactant-enhanced remediation of organic contaminated soil and water. *Adv. Colloid Interface Sci.* **2008**, *138* (1), 24−58.
(17) Adeel, Z.; Luthy, R. G. Sorption and transport kinetics of a nonionic surfactant through an aquifer sediment. *Environ. Sci. Technol.* **1995**, *29* (4), 1032−1042.
(18) Wang, P.; Keller, A. A. Particle-Size Dependent Sorption and Desorption of Pesticides within a Water− Soil− Nonionic Surfactant System. *Environ. Sci. Technol.* **2008**, *42* (9), 3381−3387.
(19) Jones-Hughes, T.; Turner, A. Sorption of ionic surfactants to estuarine sediment and their influence on the sequestration of phenanthrene. *Environ. Sci. Technol.* **2005**, *39* (6), 1688−1697.
(20) Adeel, Z.; Luthy, R. G. *Concentration-Dependent Regimes in Sorption and Transport of a Nonionic Surfactant in Sand−Aqueous Systems*; American Chemical Society, 1995.
(21) Edwards, D. A.; Adeel, Z.; Luthy, R. G. Distribution of nonionic surfactant and phenanthrene in a sediment/aqueous system. *Environ. Sci. Technol.* **1994**, *28* (8), 1550−1560.
(22) Ying, G.-G. Fate, behavior and effects of surfactants and their degradation products in the environment. *Environ. Int.* **2006**, *32* (3), 417−431.
(23) Somasundaran, P.; Krishnakumar, S. Adsorption of surfactants and polymers at the solid-liquid interface. *Colloids Surf., A* **1997**, *123*, 491−513.
(24) Wesson, L. L.; Harwell, J. H. Surfactant adsorption in porous media. *Surfactants: fundamentals and applications in the petroleum industry* **2000**, 121−158.
(25) Al-Hajri, S.; Mahmood, S.; Abdulelah, H.; Akbari, S. An overview on polymer retention in porous media. *Energies* **2018**, *11* (10), 2751.
(26) Karagunduz, A.; Young, M. H.; Pennell, K. D. Influence of surfactants on unsaturated water flow and solute transport. *Water Resour. Res.* **2015**, *51* (4), 1977−1988.
(27) Urano, K.; Saito, M.; Murata, C. Adsorption of surfactants on sediments. *Chemosphere* **1984**, *13* (2), 293−300.
(28) Matthijs, E.; De Henau, H. Adsorption and desorption of LAS. *Tenside Detergents* **1985**, *22* (6), 299−304.
(29) Abe, I.; Hayashi, K.; Tatsumoto, H.; Kitagawa, M.; Hirashima, T. The relation between activated carbon adsorption and water quality indexes. *Water Res.* **1985**, *19* (9), 1191−1193.
(30) van Eijk, M. C.; Cohen Stuart, M. A. Polymer adsorption kinetics: Effects of supply rate. *Langmuir* **1997**, *13* (20), 5447−5450.
(31) Adeel, Z.; Luthy, R. G.; Edwards, D. A. Modeling Transport of Multiple Organic Compounds: Segregated Transport-Sorption/Solubilization Numerical Technique. *Water Resour. Res.* **1995**, *31* (8), 2035−2045.
(32) Dror, Y.; Cohen, Y.; Yerushalmi-Rozen, R. Structure of gum arabic in aqueous solution. *J. Polym. Sci., Part B: Polym. Phys.* **2006**, *44* (22), 3265−3271.
(33) Pennell, K. D.; Adinolfi, A. M.; Abriola, L. M.; Diallo, M. S. Solubilization of dodecane, tetrachloroethylene, and 1, 2-dichlorobenzene in micellar solutions of ethoxylated nonionic surfactants. *Environ. Sci. Technol.* **1997**, *31* (5), 1382−1389.
(34) Wang, Y.; Li, Y.; Costanza, J.; Abriola, L. M.; Pennell, K. D. Enhanced mobility of fullerene (C60) nanoparticles in the presence of stabilizing agents. *Environ. Sci. Technol.* **2012**, *46* (21), 11761−11769.
(35) Standard D2434-68. Standard Test Method for Permeability of Granular Soils (Constant Head). ASTM International: West Conshohocken, PA, 2006.
(36) Becker, M. D.; Wang, Y.; Paulsen, J. L.; Song, Y.-Q.; Abriola, L. M.; Pennell, K. D. In situ measurement and simulation of nanomagnetite mobility in porous media subject to transient salinity. *Nanoscale* **2015**, *7* (3), 1047−1057.
(37) Toride, N.; Leij, F.; Van Genuchten, M. T. *The CXTFIT code for estimating transport parameters from laboratory or field tracer experiments*; 1995; Vol. 2.
(38) Sabatini, D. A.; Austin, T. Characteristics of Rhodamine WT and Fluorescein as adsorbing ground-water tracers. *Groundwater* **1991**, *29* (3), 341−349.

(39) Howes, A.; Radke, C. Monte Carlo simulations of Lennard-Jones nonionic surfactant adsorption at the liquid/vapor interface. *Langmuir* **2007**, *23* (4), 1835−1844.
(40) Li, Y.; Wang, Y.; Pennell, K. D.; Abriola, L. M. Investigation of the transport and deposition of fullerene (C60) nanoparticles in quartz sands under varying flow conditions. *Environ. Sci. Technol.* **2008**, *42* (19), 7174−7180.
(41) Sanchez, C.; Schmitt, C.; Kolodziejczyk, E.; Lapp, A.; Gaillard, C.; Renard, D. The acacia gum arabinogalactan fraction is a thin oblate ellipsoid: a new model based on small-angle neutron scattering and ab initio calculation. *Biophys. J.* **2008**, *94* (2), 629−639.
(42) Taylor, T. P.; Pennell, K. D.; Abriola, L. M.; Dane, J. H. Surfactant enhanced recovery of tetrachloroethylene from a porous medium containing low permeability lenses: 1. Experimental studies. *J. Contam. Hydrol.* **2001**, *48* (3−4), 325−350.
(43) Ko, C.-H.; Elimelech, M. The "shadow effect" in colloid transport and deposition dynamics in granular porous media: measurements and mechanisms. *Environ. Sci. Technol.* **2000**, *34* (17), 3681−3689.
(44) Taghavy, A.; Abriola, L. M. Modeling reactive transport of polydisperse nanoparticles: assessment of the representative particle approach. *Environ. Sci.: Nano* **2018**, *5* (10), 2293−2303.
(45) Hu, Z.; Zhao, J.; Gao, H.; Nourafkan, E.; Wen, D. Transport and deposition of carbon nanoparticles in saturated porous media. *Energies* **2017**, *10* (8), 1151.
(46) Torkzaban, S.; Bradford, S. A.; Walker, S. L. Resolving the coupled effects of hydrodynamics and DLVO forces on colloid attachment in porous media. *Langmuir* **2007**, *23* (19), 9652−9660.

https://dx.doi.org/10.1021/acs.est.0c00123
Environ. Sci. Technol. 2020, 54, 4912−4921